Supporting Information

Amphiphilic Acetylacetone-Based Carbon Dots

Sergei A. Cherevkov,[a ǂ] Evgeniia A. Stepanidenko,[a ǂ] Mikhail D. Miruschenko,[a] Andrei M. Zverkov,[a] Alexander M. Mitroshin,[a,b] Igor V. Margaryan,[a] Igor G. Spiridonov,[a] Denis V. Danilov,[c] Aleksandra V. Koroleva,[c] Evgeniy V. Zhizhin,[c] Marina V. Baidakova,[d] Roman V. Sokolov,[d] Maria A. Sandzhieva,[e] Elena V. Ushakova,[a,f]* Andrey L. Rogach[f,g]

a. *International Research and Education Centre for Physics of Nanostructures, ITMO University, 197101 Saint Petersburg, Russia*
b. *Institute of Macromolecular Compounds Russian Academy of Sciences, Saint Petersburg 199004, Russia*
c. *Research Park, Saint Petersburg State University, 199034 Saint Petersburg, Russia*
d. *Ioffe Institute, 194021 Saint Petersburg, Russia*
e. *School of Physics and Engineering, ITMO University, 197101 Saint Petersburg, Russia*
f. *Department of Materials Science and Engineering, and Centre for Functional Photonics (CFP), City University of Hong Kong, Hong Kong SAR 999077, P. R. China*
g. *IT4Innovations, VSB – Technical University of Ostrava, 17. listopadu 2172/15, 70800 Ostrava-Poruba, Czech Republic*

*Corresponding author: elena.ushakova@itmo.ru

ǂ Equal contribution

Materials

Benzoic acid (BA, ≥99.5%), acetylacetone (≥99%), and ethylenediamine (EDA, ≥99.5%), polystyrene (PS) were obtained from Sigma-Aldrich (Darmstadt, Germany). Toluene (>99.5%), chloroform (>99.8%), acetone (>99.8%), acetonitrile (>99.8%), chlorobenzene (>99.5%), isopropanol (>99.8%), and glycerin (>98.5%) were purchased from Ekos-1 (Moscow, Russia). PVK (polyvinylcarbazole), PEDOT:PSS (poly(3,4 ethylenedioxythiophene):poly(styrenesulfonate)), and PolyTPD were obtained from Ossila (Sheffield, England). TBPi (2,2',2''-(1,3,5-benzinetriyl)-tris(1 phenyl 1 H benzimidazole)) was obtained from Lumtec (New Taipei City, Taiwan). Glass substrates with an indium tin oxide (ITO) layer were obtained from Kaivo LTD (Zhuhai, Guangdong, China). All reagents were of analytical grade and used directly without further purification. Deionized water was produced through a Millipore water purification system (Milli-Q, Millipore) and used throughout the study.

Dialysis procedure

To purify the obtained crude product from possible contaminants including small molecules, the stock solution was firstly passed through a syringe filter (200 nm) to discard large agglomerates. Next, 5 mL of the stock solution was filled into in a dialysis bag with a molecular weight cut-off of 7 kDa, and placed into 700 mL of dialysate. For the first purification step, a mixture of water with isopropanol was used as a dialysate for better extruding both hydrophobic and hydrophilic moieties. The dialysate was changed no less than 10 times. Thin-film chromatography was then carried out to check for the presence of any possible moieties still present in the purified solution. As can be seen from Figure S1, the purified solution doesn't contain any molecular moieties.

Characterization

A Libra 200FE (Zeiss, Oberkochen, Germany) transmission electron microscope (TEM) and a Solver Pro-M (NT-MDT, Moscow, Russia) atomic-force microscope (AFM) were used to study size and shape of CDs. For AFM measurements, 10 μL solutions of CDs redispersed in 2-methoxyethanol at a concentration of 18 mg/mL were spin-cast onto the mica substrates at 4000 rpm for 40 sec, and annealed at 130°C for 15 min. X-Ray photoelectron spectroscopy (XPS) measurements were performed on an Escalab 250Xi (Thermo Fisher Scientific, Waltham, MA, USA) photoelectron spectrometer with AlKα radiation (photon energy 1486.6 eV) in the constant pass energy mode at 100 eV for the survey XPS spectrum and at 50 eV for the core-level spectra of single elements, using an XPS spot size of 650 μm. X-ray diffraction (XRD) measurements were carried out on an X-ray powder diffractometer D2 Phaser (Brucker AXS GmbH, Germany), Cu-Kα, Ni filter monochromatization, LYNXEYE semiconductor linear detector (Bruker AXS) with an opening angle of 5°, 2θ-θ scanning. All spectroscopic studies were performed under an ambient atmosphere. Raman spectra were measured on an inVia (Renishaw, Wotton-under-Edge, UK) microspectrometer equipped with a 20× objective (NA = 0.4) and a 514 nm laser source. Fourier-transform infrared (FTIR) spectra were recorded on a Tenzor II infrared spectrophotometer (Bruker, Billerica, MA, U.S.) in an attenuated total reflection mode. Absorption spectra were measured using a Shimadzu UV3600 spectrophotometer (Shimadzu, Kyoto, Japan). Photoluminescence (PL) spectra and PL excitation-emission (PLE-PL) maps were recorded on a Cary Eclipse instrument (Agilent, Santa Clara, CA, USA). Time-resolved PL measurements were performed on a confocal microscope MicroTime 100 (PicoQuant, Berlin, Germany) equipped with a 3× objective (NA = 0.1) and a 405 nm pulsed diode laser. For all optical measurements, CDs were dissolved in different solvents with concentration of 0.5 mg/mL. Electroluminescence spectra of CD-LEDs were obtained using a CAS 120 spectrometer (Instrument Systems, Munich, Germany). I/V characteristics were measured using a Keithley 2401 measuring source (Keithley Instruments, Solon, Ohio, USA). PL spectra from CD-LED were taken by an LSM-710 (Zeiss, Oberkochen, Germany) laser confocal microscope with a 405 nm diode laser.

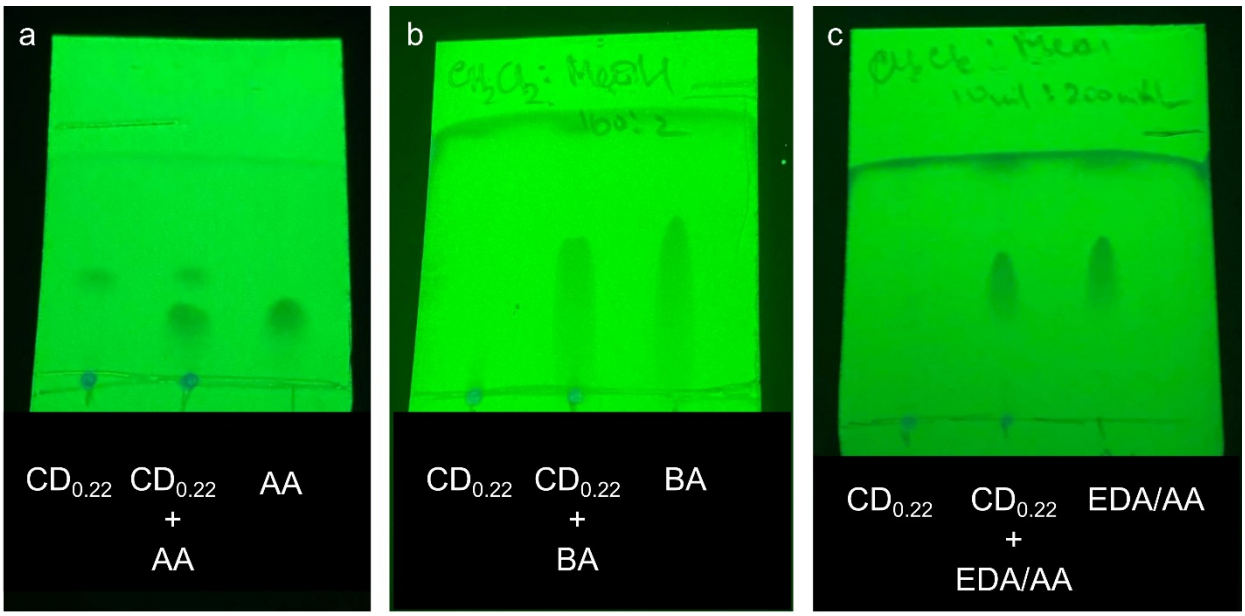

Figure S1. Photographs of thin-layer chromatography plates Sorbifill (Russia) for $CD_{0.22}$ and the precursors, taken under UV light (254 nm). (a) Comparison with acetylacetone (AA): eluent - mixture of chloroform and hexane (10:3); Retention factor (Rf) for CDs – 0.5, for AA – 0.3. (b) Comparison with benzoic acid (BA): eluent - mixture of dichloromethane and methanol (100:2); Rf for CDs – 0, for AA – 0.6. (c) Comparison with ethylenediamine in acetylacetone (EDA/AA): eluent - mixture of dichloromethane and methanol (100:2); Rf for CDs – 0, for AA – 0.7. The difference in the spots on the plates clearly shows that the purified CDs do not contain any molecular moieties or residual precursors.

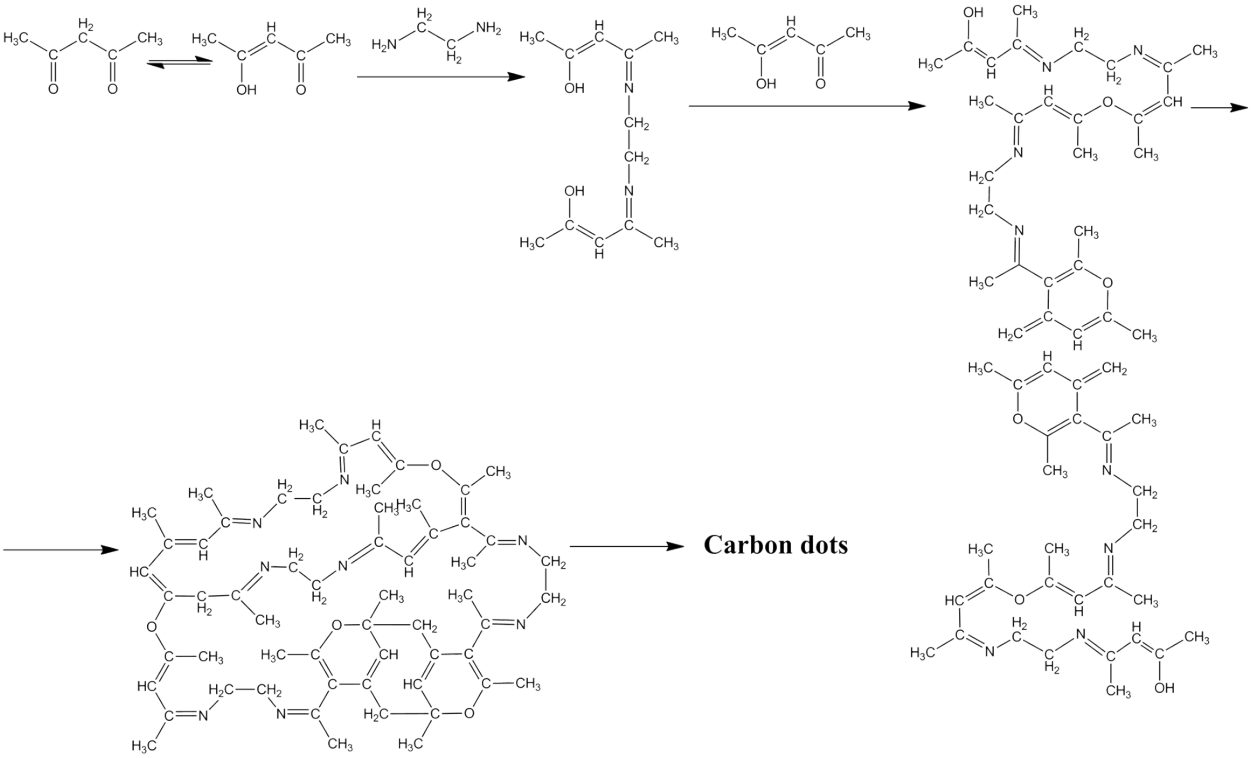

Figure S2. Possible reaction scheme for the formation of CD_{EDA} from EDA in acetylacetone.

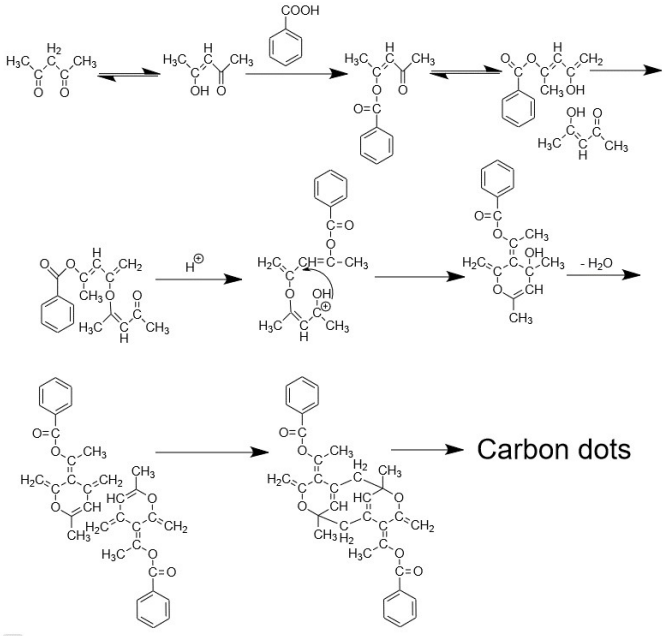

Figure S3. Possible reaction scheme for the formation of CD_{BA} from BA in acetylacetone

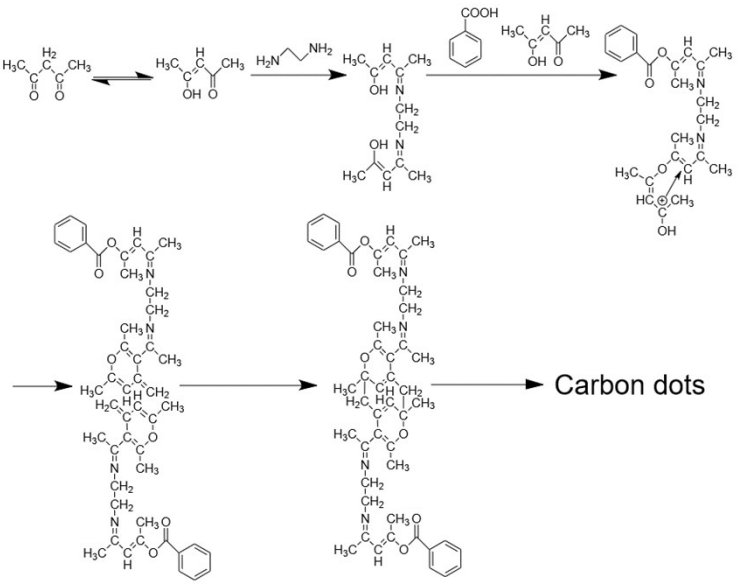

Figure S4. Possible reaction scheme for the formation of CD from BA and EDA in acetylacetone.

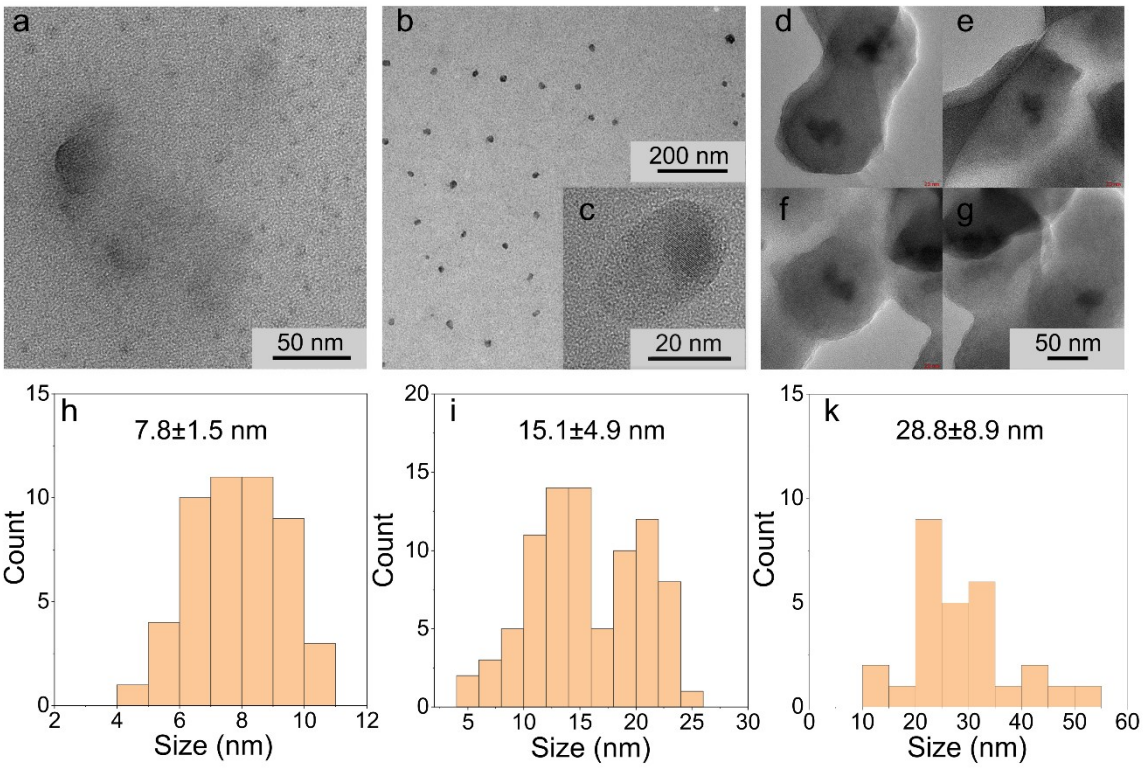

Figure S5. (a-g) TEM images of CD_{EDA} (a), $CD_{0.22}$ (b, c), and CD_{BA} (d-g). Size distributions obtained from those TEM images for CD_{EDA} (h), $CD_{0.22}$ (i), and CD_{BA} (k).

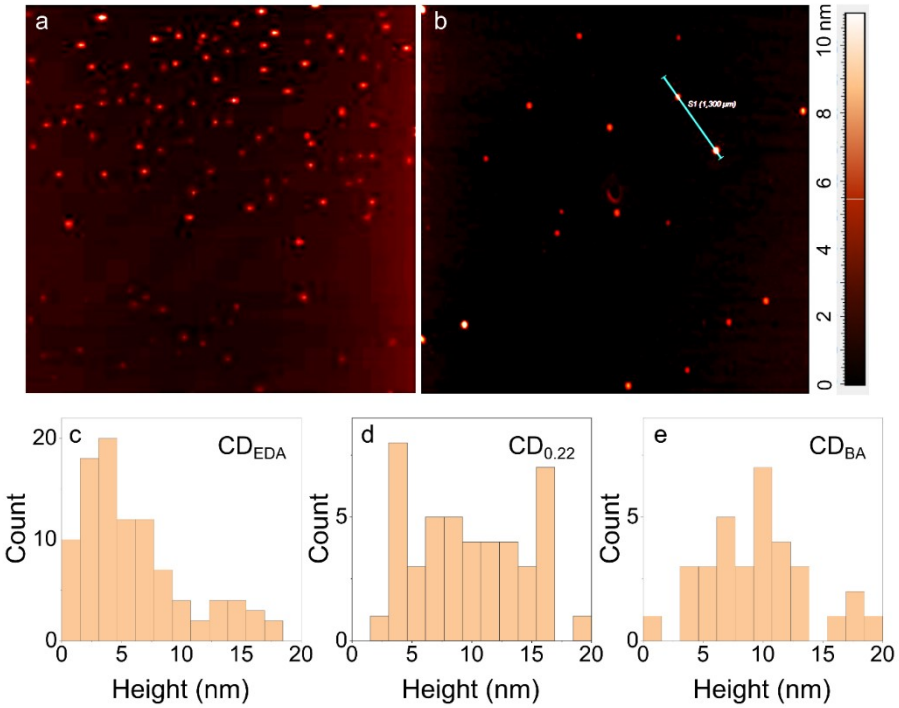

Figure S6. AFM images of CD_{EDA} (a) and CD_{BA} (b). Height distributions for CD_{EDA} (c), $CD_{0.22}$ (d), and CD_{BA} (e) determined by AFM.

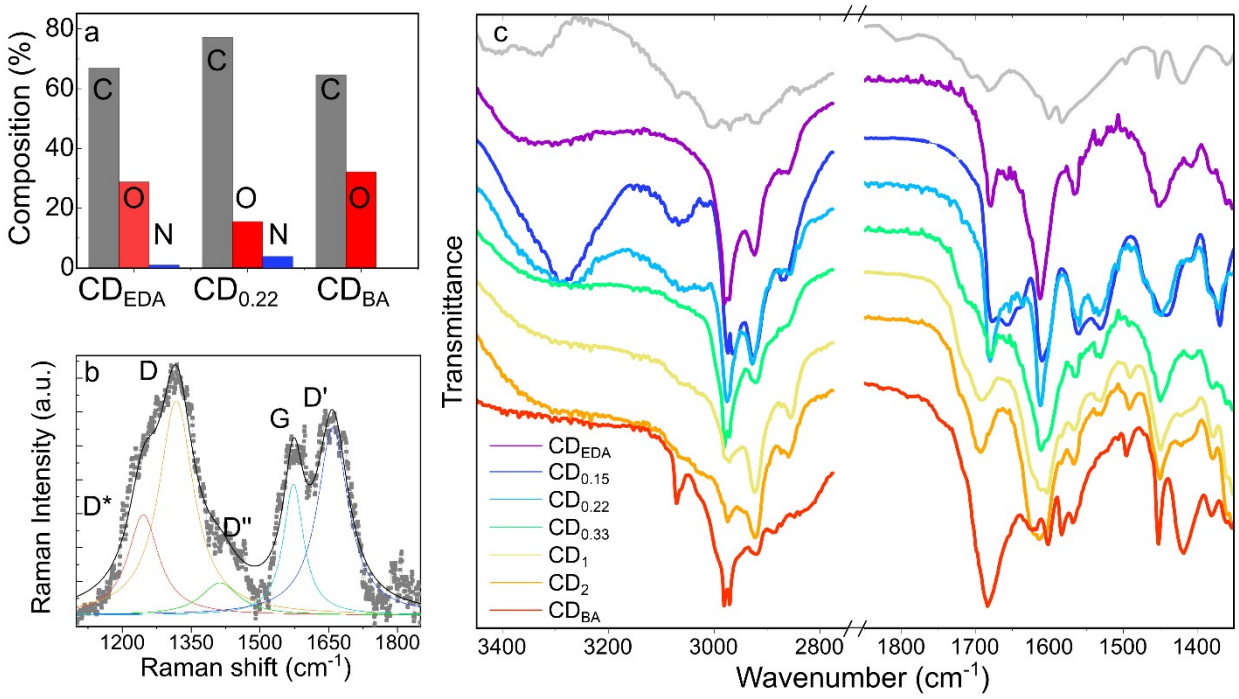

Figure S7. Chemical composition of amphiphilic CDs. (a) Atomic percentage of carbon (grey), oxygen (red), and nitrogen (blue) elements in CD_{EDA}, $CD_{0.22}$, and CD_{BA} determined from XPS measurements. (b) Raman spectrum of $CD_{0.22}$ and its deconvolution into D* (red), D (orange), D" (green), G (cyan), and D' (blue) bands typical for carbon polymorphs. (c) FTIR spectra of amphiphilic CDs; grey-color spectrum on the top represents a sum of the precursor spectra (EDA, BA, and acetylacetone).

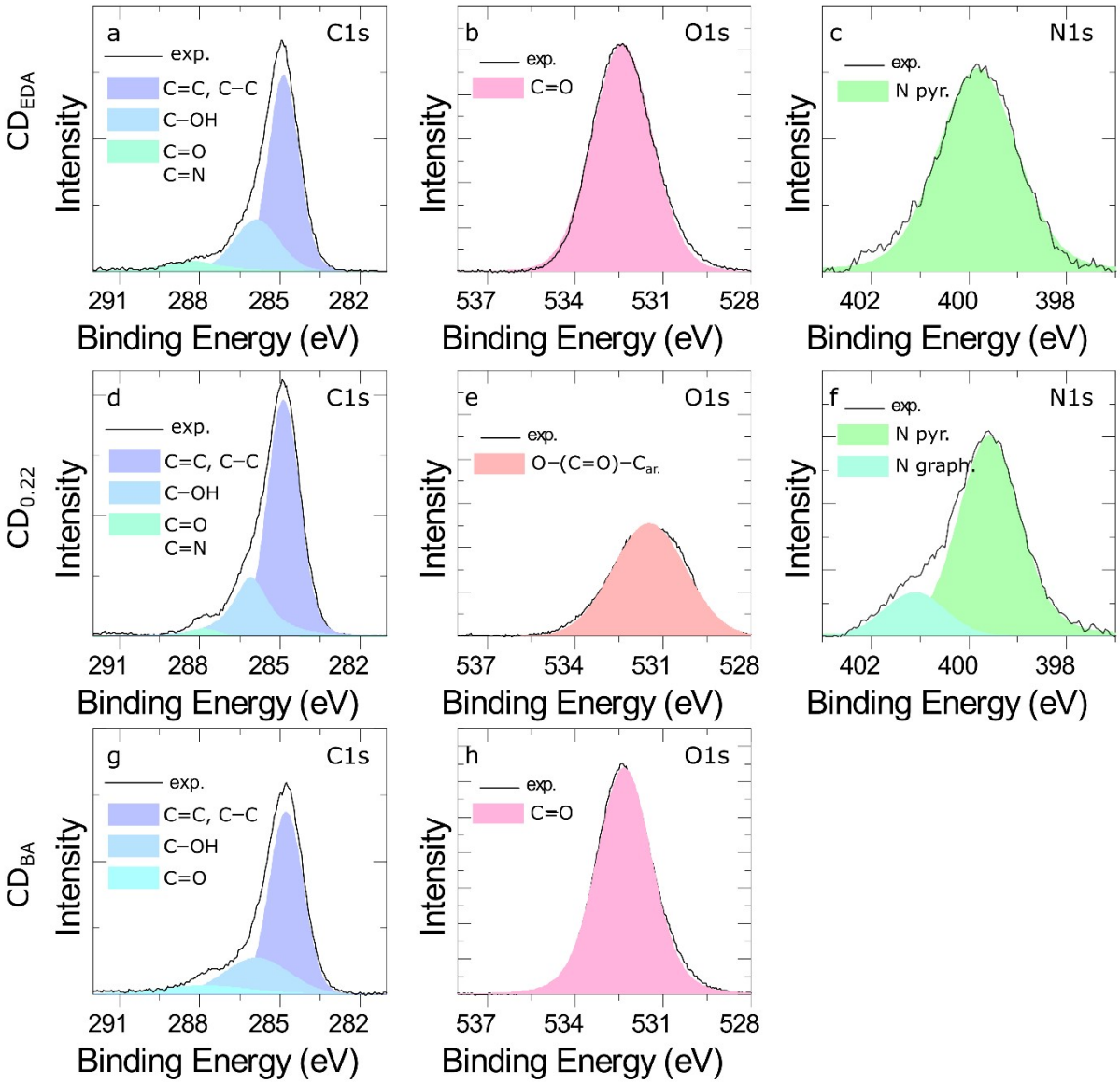

Figure S8. High resolution XPS spectra of C 1s (a, d, g), O 1s (b, e, h), and N 1s (c, f) for CD_{EDA} (a-c), $CD_{0.22}$ (d-f), and CD_{BA}(g, h). Considering the width of N 1s band, the peak can be attributed to pyridinic (398 eV) and graphitic (401 eV) N.

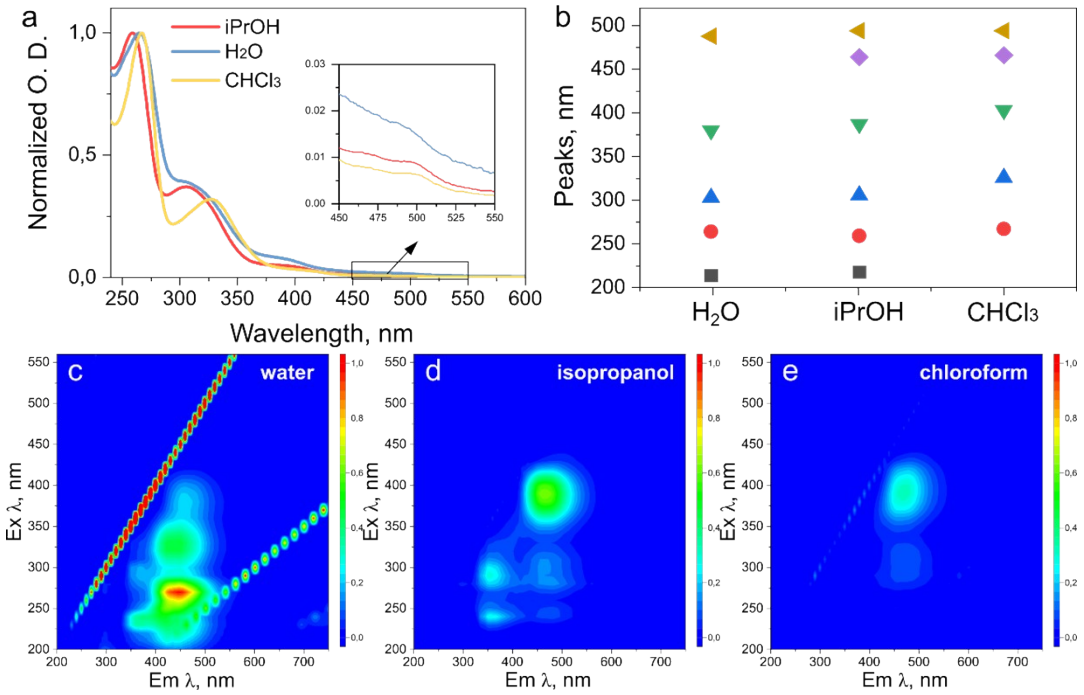

Figure S9. Optical properties of CD_{EDA}. (a) Absorption spectra, the inset shows zoom-in of the 450-550 nm spectral region; (b) peaks position, corresponding to the absorption bands Abs-1 (green triangles), Abs-2 (blue triangles), Abs-3 (red circles) from Table S1, and to absorption peaks not contributing to emission: UV absorption band (black squares) and the bands at 450-500 nm (purple diamonds and yellow triangles). (c-e) PLE-PL maps in water (c), isopropanol (d), and chloroform (e).

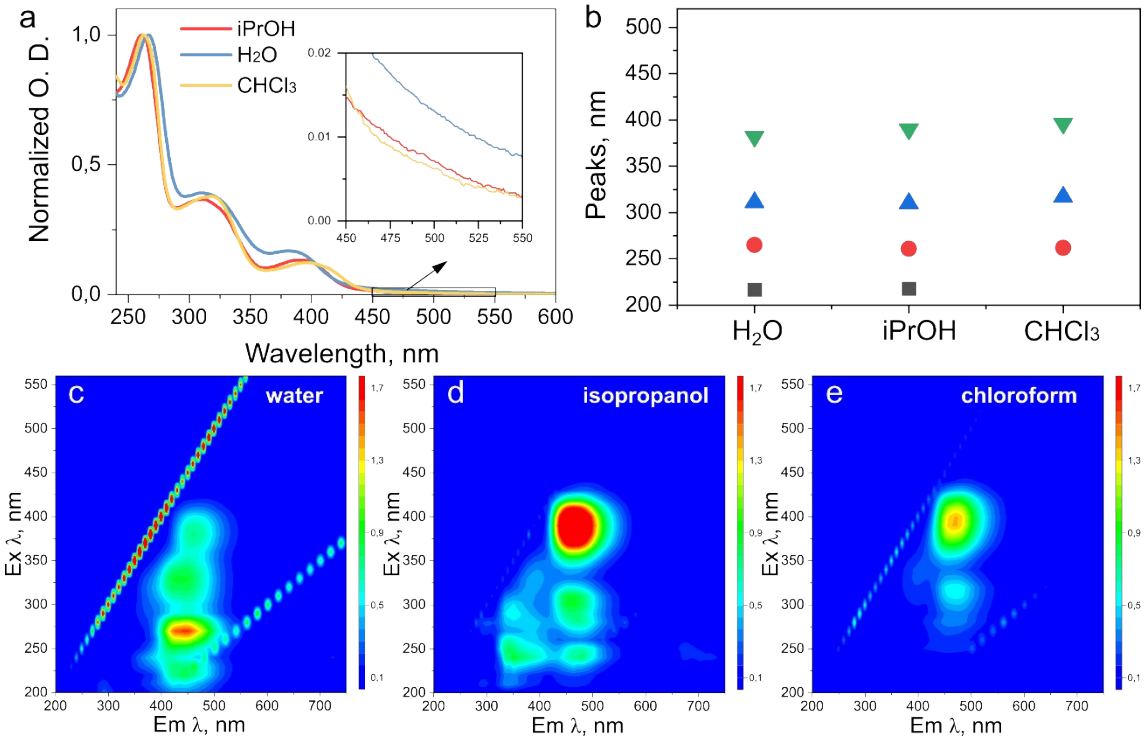

Figure S10. Optical properties of $CD_{0.15}$. (a) Absorption spectra, the inset shows zoom-in of the 450-550 nm spectral region; (b) peaks position, corresponding to the absorption bands Abs-1 (green triangles), Abs-2 (blue triangles), Abs-3 (red circles) from Table S1, and to absorption peaks not contributing to emission: UV absorption band (black squares). (c-e) PLE-PL maps in water (c), isopropanol (d), and chloroform (e).

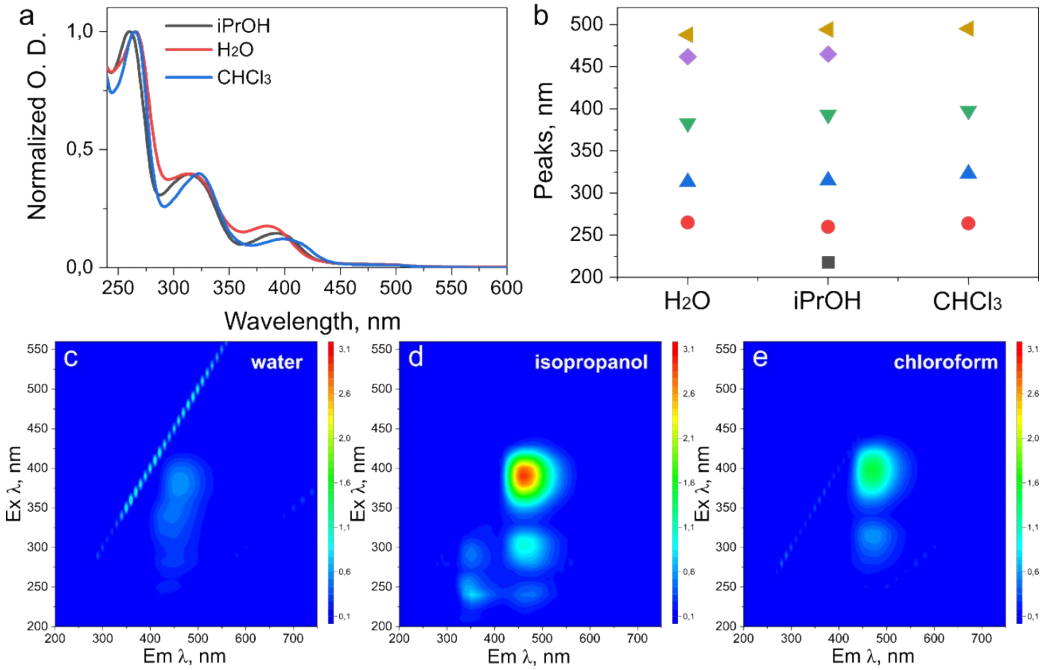

Figure S11. Optical properties of $CD_{0.22}$. (a) Absorption spectra, the inset shows zoom-in of the 450-550 nm spectral region; (b) peaks position, corresponding to the absorption bands Abs-1 (green triangles), Abs-2 (blue triangles), Abs-3 (red circles) from Table S1, and to absorption peaks not contributing to emission: UV absorption band (black squares) and the bands at 450-500 nm (purple diamonds and yellow triangles). (c-e) PLE-PL maps in water (c), isopropanol (d), and chloroform (e).

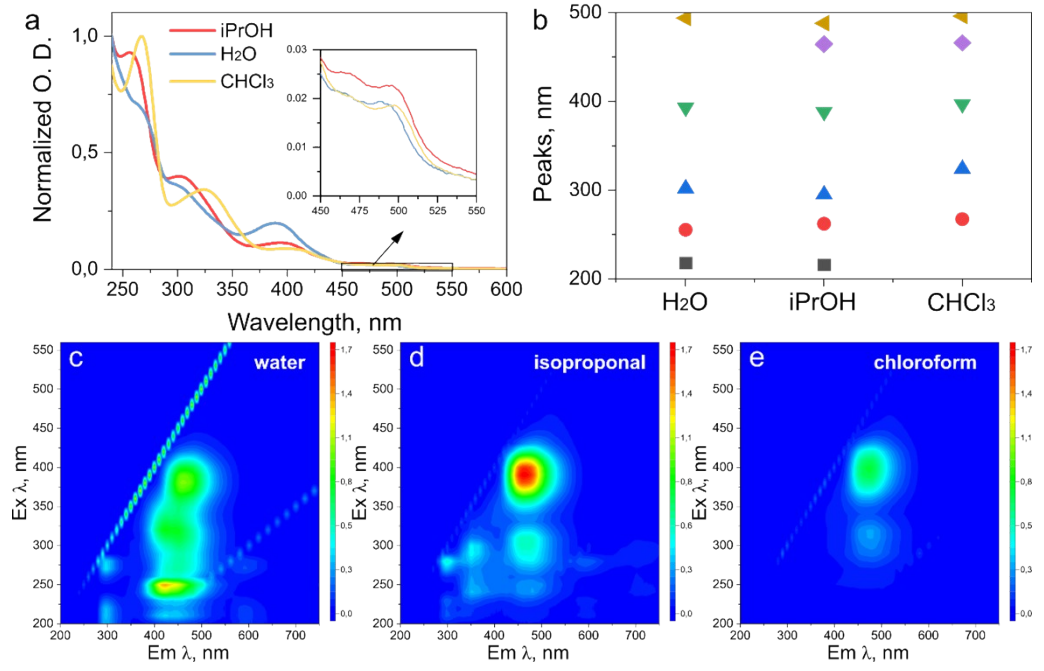

Figure S12. Optical properties of $CD_{0.33}$. (a) Absorption spectra, the inset shows zoom-in of the 450-550 nm spectral region; (b) peaks position, corresponding to the absorption bands Abs-1 (green triangles), Abs-2 (blue triangles), Abs-3 (red circles) from Table S1, and to absorption peaks not contributing to emission: UV absorption band (black squares) and the bands at 450-500 nm (purple diamonds and yellow triangles). (c-e) PLE-PL maps in water (c), isopropanol (d), and chloroform (e).

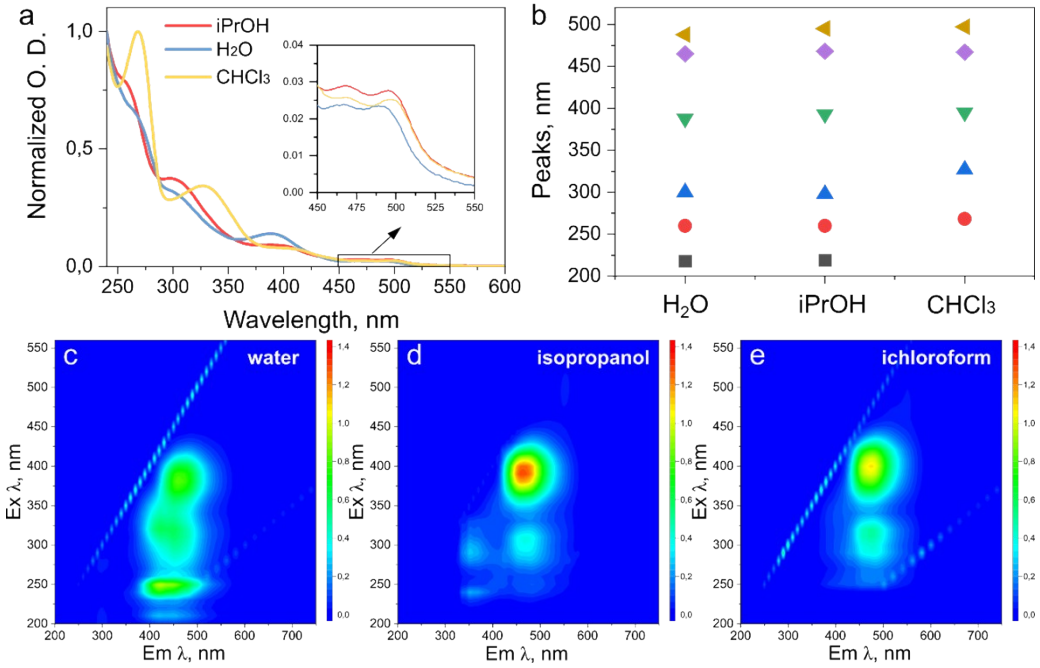

Figure S13. Optical properties of CD_1. (a) Absorption spectra, the inset shows zoom-in of the 450-550 nm spectral region; (b) peaks position, corresponding to the absorption bands Abs-1 (green triangles), Abs-2 (blue triangles), Abs-3 (red circles) from Table S1, and to absorption peaks not contributing to emission: UV absorption band (black squares) and the bands at 450-500 nm (purple diamonds and yellow triangles). (c-e) PLE-PL maps in water (c), isopropanol (d), and chloroform (e).

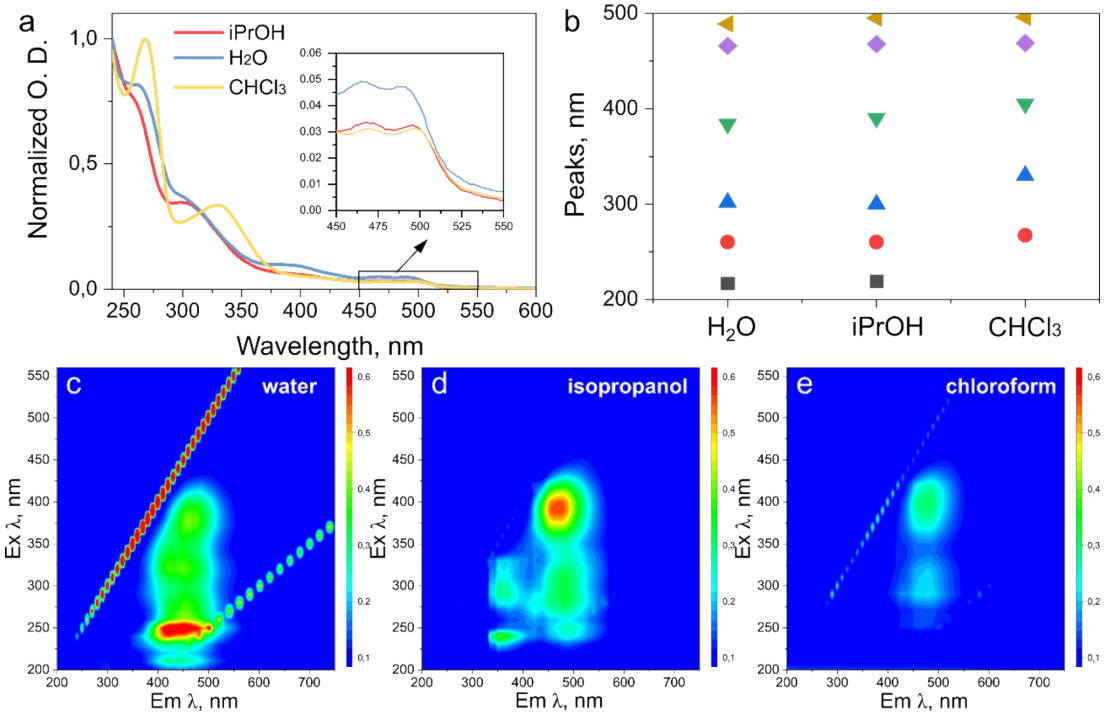

Figure S14. Optical properties of CD_2. (a) Absorption spectra, the inset shows zoom-in of the 450-550 nm spectral region; (b) peaks position, corresponding to the absorption bands Abs-1 (green triangles), Abs-2 (blue triangles), Abs-3 (red circles) from Table S1, and to absorption peaks not contributing to emission: UV absorption band (black squares) and the bands at 450-500 nm (purple diamonds and yellow triangles). (c-e) PLE-PL maps in water (c), isopropanol (d), and chloroform (e).

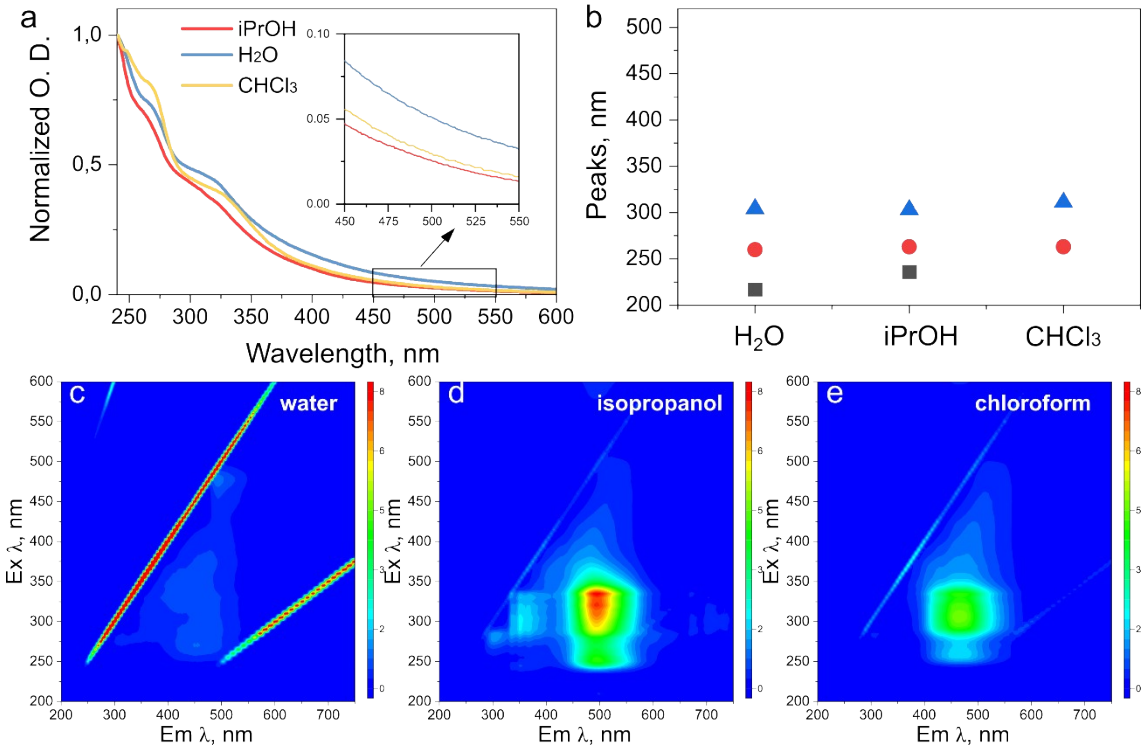

Figure S15. Optical properties of CD_{BA}. (a) Absorption spectra, the inset shows zoom-in of the 450-550 nm spectral region; (b) peaks position, corresponding to the absorption bands Abs-2 (blue triangles) and Abs-3 (red circles) from Table S1, and to absorption peaks not contributing to emission: UV absorption band (black squares). (c-e) PLE-PL maps in water (c), isopropanol (d), and chloroform (e).

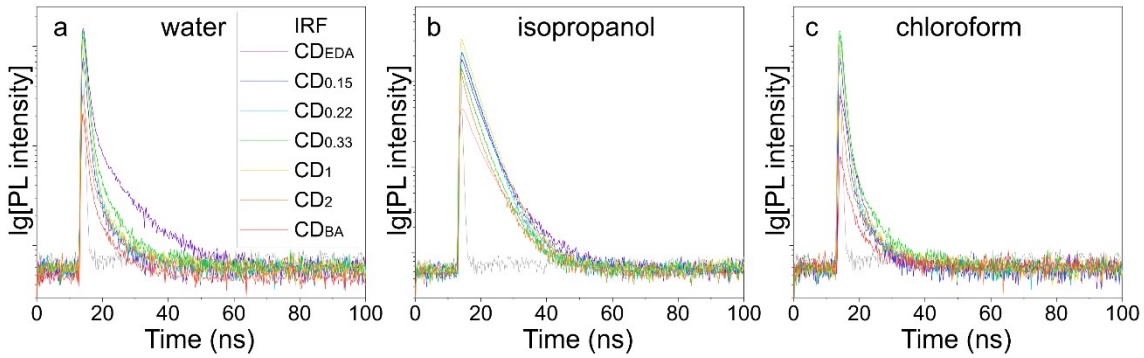

Figure S16. PL decays of the CD samples listed on the frame (a) in water (a), isopropanol (b), and chloroform (c).

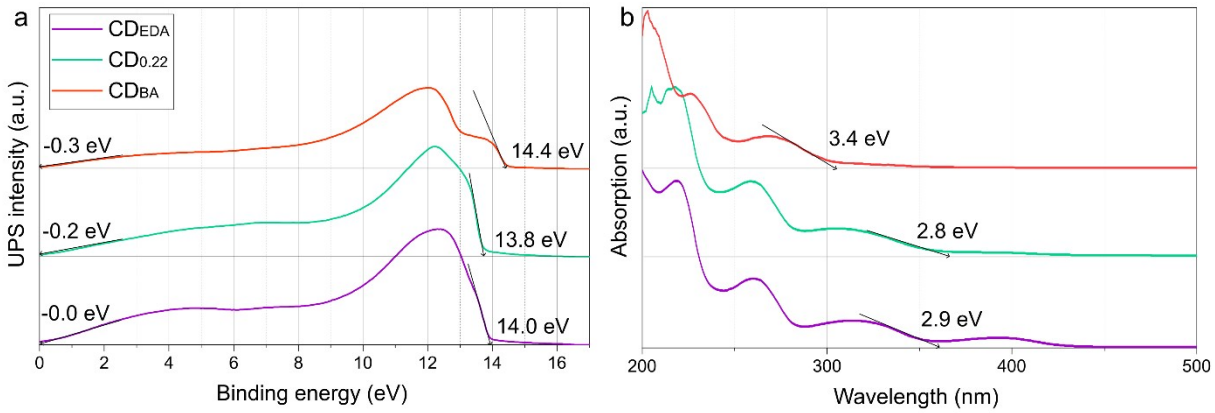

Figure S17. (a) UPS spectra of CD_{EDA}, $CD_{0.22}$, and CD_{BA}. Arrows show the tangent of the curves used to determine the spectral width. (b) Absorption spectra of CD_{EDA}, $CD_{0.22}$, and CD_{BA}. Arrows show the tangent of the curves used to determine the energy bandgap.

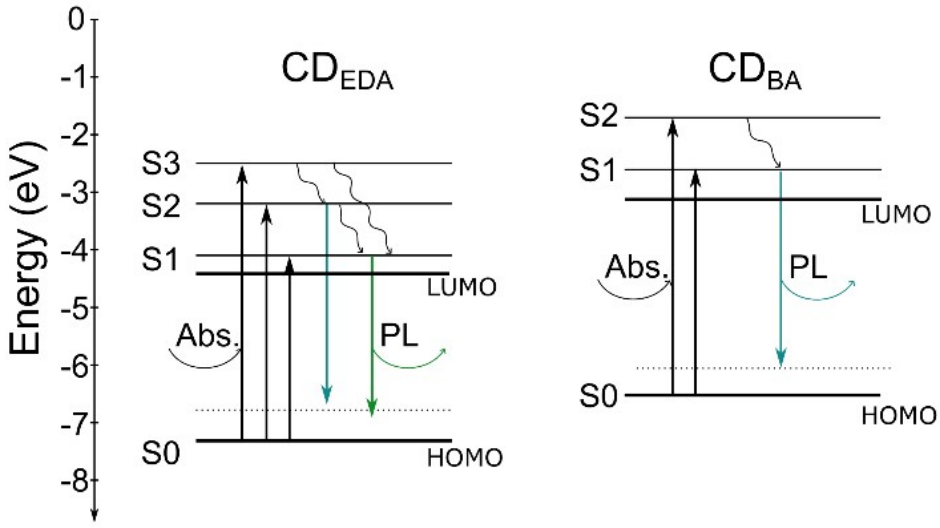

Figure S18. Suggested energy level structures of CD_{EDA} and CD_{BA}. From the optical data, one can identify excited states shown as thin black lines towards S1, S2, and S3 states for CD_{EDA}, and S1 and S2 states for CD_{BA}, which correspond to the absorption peaks listed in Table S3. Nonradiative transitions are shown by wavy lines. For CD_{EDA}, the radiative transitions of the two emissive centers corresponding to PL-1 and PL-2 in Table S3 are shown by colored arrows from the S2 and S3 energy levels, respectively. For CD_{BA}, only one radiative transition is observed from the S2 excited level.

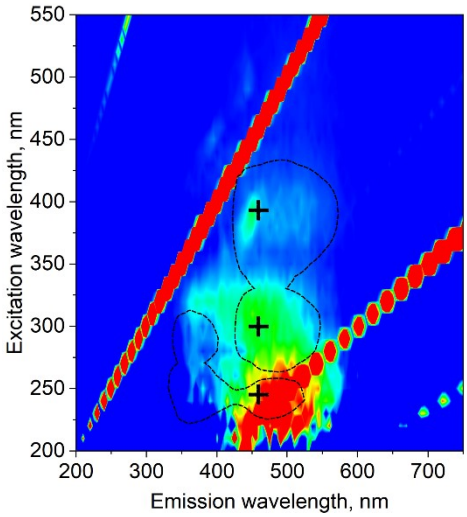

Figure S19. PLE-PL map of the $CD_{0.22}$@PVK film. An area shown by dashed curve represents several emissive centers observed for $CD_{0.22}$ in isopropanol, with the maxima shown by the crosses.

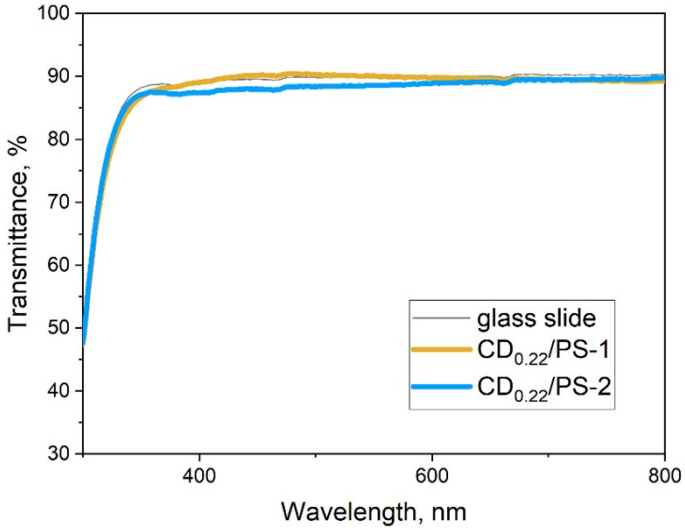

Figure S20. Transmission spectra of $CD_{0.22}$/PS-1 (orange line), $CD_{0.22}$/PS-2 (blue line), and glass slide (grey line).

Table S1. Comparison of synthetic and optical parameters of amphiphilic CDs, based on literature data and for those fabricated in this work.

CD precursors	Synthesis method *	Solvents in which CDs are soluble	Abs peak, nm	PL peak, nm	Max. PLQY, %	Reference
Paraplast, dodecanthiol in toluene	HI, 70 °C, 3h	Toluene	285	450	N/A	[1]
Rhodamine B, ethanol, Polyethylene glycol	ST, 200 °C, 20 h	petroleum ether – water	395	495	22.85	[2]
Dodecylamine in chlorobenzene	HI, 6-48 h	toluene – DMSO	N/A	486	10.83	[3]
1-[Bis(dimethylamino)methylene]-1H-1,2,3-triazolo[4,5-b]pyridinium 3-oxide hexafluorophosphate	ST, 150 °C, 8 h	toluene – water	350	530	20	[4]
citric acid and dodecylamine in c-hexane	ST, 160 °C, 18 h	c-hexane – methanol	432	535	33.1 (c-hexane)	[5]
Banana peel extract and phosphoric acid	Pyrolysis, 85 °C, 0.5 h	c-hexane – water	422	510 - 560	32 (butanol)	[6]
Citric acid, 4,7,10-Trioxa-1,13-tridecanediamine	MW, 700 W, 5 min	chloroform – water	300	440	29	[7]
Polyamine in ethanol	ST, 180 °C, 5 h	water, buffer solutions	345 - 365	445 - 460	N/A	[8]
2-aminophenol in ethanol	ST, 180 °C, 12 h	hexane – ethanol	430	531	N/A	[9]
Citric acid, organosilane	HT, 180 °C, 12 h	Water/organosilane	360	450	82	[10]
Citric acid, organosilane	HI, 240 °C, 1-60 min	organosilane	N/A	435 - 445	28-50	[11]
Polybasic acid, organosilane	HI, 240 °C, 1-60 min	organosilane	349	441	88**	[12]
Ethylenediamine and benzoic acid in acetylacetone	ST, 190 °C, 8 h	tetrachloromethane - water	390	460	36 (isopropanol)	This work

* HI – hot injection, ST – solvothermal, MW – microwave-assisted.

** optical parameters are given for best sample of CDs in Gel glasses.

Table S2. Amount of precursors used in the synthesis of CDs produced in this work.

Sample name	Precursors		Precursors, mmol		Molar ratio BA/EDA
	BA, g	EDA, mL	BA	EDA	
CD_{EDA}	0	0.5	0	7.5	-
$CD_{0.15}$	0.3	1.14	2.5	17.0	0.15
$CD_{0.22}$	0.3	0.76	2.5	11.4	0.22
$CD_{0.33}$	0.3	0.5	2.5	7.5	0.33
CD_1	0.3	0.17	2.5	2.5	1
CD_2	0.3	0.085	2.5	1.25	2
CD_{BA}	0.3	0	2.5	0	-

Table S3. Optical properties of CDs in isopropanol: absorption peaks position (Abs-1, Abs-2, Abs-3), PL excitation peaks position (PLE-1, PLE-2, PLE-3), and PL peaks position (PL-1, PL-2)

Sample name	Abs-3, Nm	Abs-2, nm	Abs-1, nm	PLE-3 (PL-2/PL-1), nm	PLE-2 (PL-2/PL-1), Nm	PLE-1 (PL-1), nm	PL-2, Nm	PL-1, nm
CD_{EDA}	260	305	390	240/240	290/290	390	355	465
$CD_{0.15}$	261	310	390	245/240	290/305	390	350	460
$CD_{0.22}$	260	315	395	240/240	290/300	390	350	460
$CD_{0.33}$	260	300	395	240/245	290/30	390	355	465
CD_1	260	300	395	240/248	290/305	390	350	465
CD_2	260	300	390	240/248	290/290	390	355	470
CD_{BA}	260	315	-	-	-	320	-	495

Table S4. PL lifetime (τ), PL QYs, radiative (Γ) and nonradiative (k_{nr}) recombination rates for the CDs fabricated in this work.

Sample name	Water				Isopropanol				Chloroform			
	τ, ns	PLQY, %	$\Gamma \cdot 10^9$, s^{-1}	$k_{nr} \cdot 10^9$, s^{-1}	τ, ns	PLQY, %	$\Gamma \cdot 10^9$, s^{-1}	$k_{nr} \cdot 10^9$, s^{-1}	τ, ns	PLQY, %	$\Gamma \cdot 10^9$, s^{-1}	$k_{nr} \cdot 10^9$, s^{-1}
CD_{EDA}	7.5	5	0.01	0.13	5.0	25	0.05	0.15	3.5	16	0.05	0.24
$CD_{0.15}$	4.0	6	0.02	0.24	4.3	34	0.08	0.15	2.8	21	0.08	0.28
$CD_{0.22}$	4.2	7	0.02	0.22	4.0	36	0.09	0.16	2.8	22	0.08	0.28
$CD_{0.33}$	4.5	6	0.01	0.21	4.3	25	0.06	0.18	4.7	16	0.03	0.18
CD_1	4.4	7	0.02	0.21	4.0	21	0.05	0.20	4.3	14	0.03	0.20
CD_2	5.2	5	0.01	0.18	4.6	12	0.03	0.19	4.0	8	0.02	0.23
CD_{BA}	5.6	2	0.005	0.18	4.4	7	0.02	0.22	6.3	2	0.005	0.15

Table S5. Energy level values for CD_{EDA}, $CD_{0.22}$, and CD_{BA} calculated from UPS, absorption, PLE and PL spectra.

Sample name	HOMO, eV	LUMO, eV	Energy gap, eV	Abs, eV	PLE, eV	PL, eV
CD_{EDA}	-7.3	-4.4	2.9	-2.5/3.2/4.1	-2.1/3.0/4.1	-5.6/5.7
$CD_{0.22}$	-7.2	-4.4	2.8	-2.4/3.3/4.0	-2.0/3.1/4.0	-5.5/5.8
CD_{BA}	-6.5	-3.1	3.4	-1.7/2.6	-2.6	-5.1

Table S6. Comparison of parameters of CD-based LEDs, based on the literature data and for those fabricated in this work.

CD precursors	PL QY, %	LED configuration	Maximal luminance, cd/m^2	Current efficiency, cd/A	Turn-on voltage, V	Threshold voltage, V	Color	Ref.
citric acid and diaminonaphthalene/ amination step with ammonia liquor and hydrazine	80	ITO/PEDOT:PSS/TFB/PVK:CQDs/TPBI/LiF/Al	5240	2.6	4.5-7.5	N/A	Deep-blue	[13]
citric acid and hexadecylamine in octadecene	41	ITO/PVK:CDs/TPBI/LiF/Al	569.8	N/A	8.5	N/A	Blue	[14]
Phloroglucinol in ethanol	72	ITO/PEDOT:PSS/PVK:CQDs/TPBI/Ca/Al	4762	5.1	3.1-4.3	N/A	Green	[15]
1,3,5-benzenetricarboxylic acid, guanidinium dihydrogen phosphate, and 3,4,9,10-perylenetetracarboxylic dianhydride	42.3	ITO/PEDOT:PSS/CD-organic framework/TPBI/LiF/Al	1818	4.0	3.3	N/A	Red	[16]
N,N-dimethyl-, N,N-diethyl-, and N,N-dipropyl-p-PD in DMF	86	ITO/PEDOT:PSS/Poly-TPD/PVK:CQDs/TPBI/Ca/Al	5909	3.65-3.85	3.0-3.3	N/A	Warm white	[17]
citric acid and hexadecylamine in octadecene	41	ITO/PVK:CDs/TPBI or TmPyPB/LiF/Al	455.2	N/A	N/A	8.5-9.5	White	[18]
Fenugreek seed derived	7.5	ITO/PEDOT:PSS/PVK:CDs/Bp4mPy/LiF/Al	115.4	N/A	5.8	2.5	Blue-	[19]

CDs							green	
Ethylenediamine and benzoic acid in acetylacetone	36	ITO/PEDOT:PSS/Poly-TPD/PVK:CDs/TPBI/LiF/Al	1716	0.2	5.2	9.7	Broad Green	**This work**

References

[1] A. Talib, S. Pandey, M. Thakur, H.F. Wu, Synthesis of highly fluorescent hydrophobic carbon dots by hot injection method using Paraplast as precursor, Materials Science and Engineering C 48 (2015) 700–703. https://doi.org/10.1016/j.msec.2014.11.058.

[2] X. Shi, X. Wang, S. Zhang, Z. Zhang, X. Meng, H. Liu, Y. Qian, Y. Lin, Y. Yu, W. Lin, H. Wang, Hydrophobic Carbon Dots Derived from Organic Pollutants and Applications in NIR Anticounterfeiting and Bioimaging, Langmuir 39 (2023) 5056–5064. https://doi.org/10.1021/ACS.LANGMUIR.3C00075/ASSET/IMAGES/LARGE/LA3C00075_0007.JPEG.

[3] K. Yin, D. Lu, L. Wang, Q. Zhang, J. Hao, G. Li, H. Li, Hydrophobic Carbon Dots from Aliphatic Compounds with One Terminal Functional Group, Journal of Physical Chemistry C 123 (2019) 22447–22456. https://doi.org/10.1021/acs.jpcc.9b04479.

[4] P. Zhao, X. Li, G. Baryshnikov, B. Wu, H. Ågren, J. Zhang, L. Zhu, One-step solvothermal synthesis of high-emissive amphiphilic carbon dots via rigidity derivation, Chem Sci 9 (2018) 1323–1329. https://doi.org/10.1039/C7SC04607C.

[5] Y. Liu, D. Sun, Z. Zhang, L. Zhang, S. Nie, J. Xiao, Y.S. Chung, H. Choi, S. Kim, C. Liu, Amphiphilic Carbon Dots with Excitation-Independent Double-Emissions, Particle and Particle Systems Characterization 37 (2020) 2000146. https://doi.org/10.1002/ppsc.202000146.

[6] S. Prakash, S. Sahu, B. Patra, A.K. Mishra, Understanding the aggregation of excitation wavelength independent emission of amphiphilic carbon dots for bioimaging and organic acid sensing, Spectrochim Acta A Mol Biomol Spectrosc 290 (2023) 122257. https://doi.org/10.1016/J.SAA.2022.122257.

[7] Y. Choi, S. Jo, A. Chae, Y.K. Kim, J.E. Park, D. Lim, S.Y. Park, I. In, Simple Microwave-Assisted Synthesis of Amphiphilic Carbon Quantum Dots from A3/B2 Polyamidation Monomer Set, ACS Appl Mater Interfaces 9 (2017) 27883–27893. https://doi.org/10.1021/ACSAMI.7B06066/ASSET/IMAGES/LARGE/AM-2017-06066E_0008.JPEG.

[8] P. Chen, X. He, Y. Hu, X.L. Tian, X.Q. Yu, J. Zhang, Spleen-Targeted mRNA Delivery by Amphiphilic Carbon Dots for Tumor Immunotherapy, ACS Appl Mater Interfaces 15 (2023) 19937–19950. https://doi.org/10.1021/acsami.3c00494.

[9] A. Mikhraliieva, O. Tkachenko, R. Freire, V. Zaitsev, Y. Xing, A. Panteleimonov, M. Strømme, T.M. Budnyak, Carbon Nanodots with Solvatochromic Photoluminescence for the Electrochemical Determination of Estrogenic Steroids, ACS Appl Nano Mater 2022 (2022) 10962–10972. https://doi.org/10.1021/ACSANM.2C02219/SUPPL_FILE/AN2C02219_SI_001.PDF.

[10] Z. Xie, Q. Du, Y. Wu, X. Hao, C. Liu, Full-band UV shielding and highly daylight luminescent silane-functionalized graphene quantum dot nanofluids and their arbitrary polymerized hybrid gel glasses, J Mater Chem C Mater 4 (2016) 9879–9886. https://doi.org/10.1039/C6TC02035F.

[11] Z. Xie, Z. Yin, Y. Wu, C. Liu, X. Hao, Q. Du, X. Xu, White Light-Emitting Diodes Based on Individual Polymerized Carbon Nanodots, Scientific Reports 2017 7:1 7 (2017) 1–9. https://doi.org/10.1038/s41598-017-12083-2.

[12] Z. Xie, F. Wang, C.-Y. Liu, Z. Xie, F. Wang, C.-Y. Liu, Organic–Inorganic Hybrid Functional Carbon Dot Gel Glasses, Advanced Materials 24 (2012) 1716–1721. https://doi.org/10.1002/ADMA.201104962.

[13] F. Yuan, Y.K. Wang, G. Sharma, Y. Dong, X. Zheng, P. Li, A. Johnston, G. Bappi, J.Z. Fan, H. Kung, B. Chen, M.I. Saidaminov, K. Singh, O. Voznyy, O.M. Bakr, Z.H. Lu, E.H. Sargent, Bright high-colour-purity deep-blue carbon dot light-emitting diodes via efficient edge amination, Nature Photonics 2019 14:3 14 (2019) 171–176. https://doi.org/10.1038/s41566-019-0557-5.

[14] J. Xu, Y. Miao, J. Zheng, Y. Yang, X. Liu, J. Xu, Y. Miao, J. Zheng, Y. Yang, X. Liu, Ultrahigh Brightness Carbon Dot–Based Blue Electroluminescent LEDs by Host–Guest Energy Transfer Emission Mechanism, Adv Opt Mater 6 (2018) 1800181. https://doi.org/10.1002/ADOM.201800181.

[15] F. Yuan, T. Yuan, L. Sui, Z. Wang, Z. Xi, Y. Li, X. Li, L. Fan, Z. Tan, A. Chen, M. Jin, S. Yang, Engineering triangular carbon quantum dots with unprecedented narrow bandwidth emission for multicolored LEDs, Nat Commun 9 (2018) 1–11. https://doi.org/10.1038/s41467-018-04635-5.

[16] Y. Shi, Z. Wang, T. Meng, T. Yuan, R. Ni, Y. Li, X. Li, Y. Zhang, ao Tan, S. Lei, L. Fan, Red Phosphorescent Carbon Quantum Dot Organic Framework-Based Electroluminescent Light-Emitting Diodes Exceeding 5% External Quantum Efficiency, J. Am. Chem. Soc 143 (2021) 18941–18951. https://doi.org/10.1021/jacs.1c07054.

[17] H. Jia, Z. Wang, T. Yuan, F. Yuan, X. Li, Y. Li, Z. Tan, L. Fan, S. Yang, Electroluminescent Warm White Light-Emitting Diodes Based on Passivation Enabled Bright Red Bandgap Emission Carbon Quantum Dots, Advanced Science 6 (2019) 1900397. https://doi.org/10.1002/ADVS.201900397.

[18] J. Xu, Y. Miao, J. Zheng, H. Wang, Y. Yang, X. Liu, Carbon dot-based white and yellow electroluminescent light emitting diodes with a record-breaking brightness, Nanoscale 10 (2018) 11211–11221. https://doi.org/10.1039/C8NR01834K.

[19] N. Urushihara, T. Hirai, A. Dager, Y. Nakamura, Y. Nishi, K. Inoue, R. Suzuki, M. Tanimura, K. Shinozaki, M. Tachibana, Blue-Green Electroluminescent Carbon Dots Derived from Fenugreek Seeds for Display and Lighting Applications, ACS Appl Nano Mater 4 (2021) 12472–12480. https://doi.org/10.1021/acsanm.1c02977.